Li Atoms Attached to Helium Nanodroplets

ALBERTO HERNANDO,[1] RICARDO MAYOL,[1] MARTÍ PI,[1] MANUEL BARRANCO,[1] IOANNIS S. K. KERKINES,[2] ARISTIDES MAVRIDIS[3]

[1]*Departament ECM, Facultat de Física, and IN[2]UB, Universitat de Barcelona, Diagonal 647, 08028 Barcelona, Spain*
[2]*Theoretical and Physical Chemistry Institute, The National Hellenic Research Foundation, 48 Vassileos Constantinou Ave., Athens 11635, Greece*
[3]*Physical Chemistry Laboratory, Department of Chemistry, National and Kapodistrian University of Athens, 15710 Zografou, Athens, Greece*

Received 15 December 2009; accepted 1 February 2010
Published online 25 May 2010 in Wiley Online Library (wileyonlinelibrary.com).
DOI 10.1002/qua.22636

ABSTRACT: We have studied helium drops doped with Li atoms within finite-range density functional theory using Li–He pair potentials obtained by the multireference configuration interaction method combined with augmented core-valence correlation consistent basis sets of quintuple-zeta quality. The absorption spectrum of Li around the $2p \leftarrow 2s$ transition has been determined by a semiclassical approach, and by the Fourier analysis of the time-correlation function of the Li atom in the full three-dimensional $^2\Pi_{1/2}$, $^2\Pi_{3/2}$, and $^2\Sigma_{1/2}$ potentials generated by its pairwise interaction with the helium droplet. We show that the bound–bound contribution to the absorption line is red-shifted and more pronounced in Li@^{4}He$_N$ than in Li@^{3}He$_N$, for which it is blue-shifted instead, in accordance with experiments. This fact is related to the experimental appearance of a red-shifted shoulder in the absorption line of Li attached to ^{4}He drops that is absent when it is attached to ^{3}He drops. Int J Quantum Chem 111: 400–405, 2011

Key words: doped helium droplets; electronic spectroscopy; density functional theory

Correspondence to: R. Mayol; e-mail: ricardo@ecm.ub.es
Contract grant sponsor: DGI, Spain(FEDER).
Contract grant number: FIS2008-00421/FIS.
Contract grant sponsor: Generalitat de Catalunya.
Contract grant number: 2009SGR1289.

Introduction

Superfluid droplets made of ^{4}He atoms are an ideal matrix for spectroscopic studies at low temperatures. Because those made of ^{3}He atoms are normal fluid droplets at experimental temperatures [1], the possibility to compare both systems may contribute to shed light on the quantum nature of Bose and Fermi systems [2].

Alkali atoms are weakly bound to helium droplets and reside in dimples on the droplet surface. This has been established by electronic spectroscopy, which reveals the shift and width of the electronic transitions of the attached atom, the key observables to determine the position of the impurity in a helium droplet, as shown, for example, in [3–6] and references therein.

Several experimental and theoretical works have described the main features of the absorption spectrum of alkali atoms on helium droplets [7–14]. In particular, Monte Carlo (MC) calculations of ^{4}He droplets doped with the lighter Li, Na, and K alkali atoms are available and have been used to obtain their dipole absorption spectrum [13]. These MC studies are limited to a few hundred helium atoms—in the case of ^{3}He droplets these studies are limited to a few 10ths at most [15, 16]. So far, only density functional (DF) methods [17] have been able to describe large drops, made of several thousand atoms, as those addressed in the experiments. We want to stress that only calculations for large drops may allow for a sensible comparison with experiments, as otherwise finite size effects obscure the comparison. Surface curvature is one such effect, very relevant when the impurity sits at the drop surface.

To determine the shape of the absorption line, MC and DF methods are applied in conjunction with some approximations, like the diatomics-in-molecules (DIM) assumption [18], the Franck-Condon principle and an atomic pairwise approximation for the drop-impurity interaction, see, for example, [13, 19]. Usually, a semiclassical average on the states accessible from the ground state by a dipole excitation is carried out, instead of the often technically unfeasible Fourier transform of the time-correlation function of the dopant atom moving in the potential energy surfaces (PES) obtained from the helium-excited impurity potentials. The price one has to pay for this average is the washing out of details in the absorption spectrum that may be relevant, in particular because they appear for ^{4}He and not for ^{3}He droplets.

In this work, we complete the analysis of the absorption spectrum of the lightest alkali atoms in helium droplets (see [20] for Na) presenting the results obtained for Li using the Fourier transform of the time-correlation function. We reproduce a key experimental feature, namely, that the main absorption peak of Li@^{4}He$_N$ is red-shifted with respect of that in the gas phase, whereas it is blue-shifted for Li@^{3}He$_N$ [10, 12]. We have also found a more pronounced bound–bound structure in the former than in the later, which we are prone to identify as the red-shifted shoulder observed in the absorption of Li in ^{4}He droplets, although the agreement with the experiment is only qualitative.

Method

We have used the density functional $\mathcal{E}$ of [21] for ^{4}He, and of [22] for ^{3}He, together with, the Li–He pair potentials of [23], with more dense sampling of the repulsive region similar to the Li-rare gas potentials obtained in [24]. Specifically, for the $X^2\Sigma$ potential the region between 6.35 and 25.0 Å has been thoroughly recalculated, with emphasis on the Li-He distances between 6.35 and 10.5 Å. Similarly, the excited $^2\Sigma$ state has been sampled in more detail in the 5.0–8.0 Å and 9.0–20.0 Å regions. For consistency with the rest of the curves published in [23], the new points have been calculated at the singles and doubles multireference configuration interaction (MRCI) level, with a core-valence quintuple-zeta basis set, augmented with diffuse functions on both Li and He (=aug(Li+He)-cc-pCV5Z) consisting of 261 spherical Gaussian functions [$(11s10p8d6f4g2h)_{Li}/(6s5p4d3f2g)_{He}$] [25, 26]. As in [23], basis set superposition errors (BSSE) have been calculated and corrected for along all calculated points.

To facilitate the use of these potentials, we have fit them (by simulated annealing) to an analytical expression of the kind [27]

$$V_{\mathrm{Li-He}}(r) = Ae^{-\alpha r-\beta r^2} - F(r)\times\left(\frac{C_6}{r^6}+\frac{C_{10}}{r^{10}}+\frac{C_{12}}{r^{12}}\right) \tag{1}$$

$$F(r) = \begin{cases} e^{-(1-D/r)^2} & r < D \\ 1 & r \geq D \end{cases}$$

The parameters are given in Table I. Using them, one obtains $V_{\mathrm{Li-He}}(r)$ in K when the distance r is

TABLE I
Parameters of the fit to the calculated Li-He pair potentials.

	$X^2\Sigma$	$^2\Pi$	$^2\Sigma$
A	1.6725×10^4	6.2669×10^5	8.6936×10^5
α	0.42685	0	1.6978
β	0.19706	2.8981	0
D	13.988	4.5734	21.456
C_6	1.5992×10^5	1.9521×10^5	0
C_{10}	0	3.7221×10^6	7.0088×10^3
C_{12}	3.2761×10^{10}	0	1.7527×10^{12}

expressed in Å. The resulting fits are shown in Figure 1.

In our approach, the energy of the Li–He system is written as a functional of the Li wave function $\Psi^{gs}(\mathbf{r})$ and the helium atomic density $\rho(\mathbf{r})$. For ^{3}He, we have used a Thomas-Fermi approximation to express the kinetic energy density as a function of $\rho(\mathbf{r})$ and its gradient [10]. This is justified for the large number of ^{3}He atoms in the drop. Within the pair potential approximation, we write the energy of the system as

$$E = \int d\mathbf{r}\mathcal{E}[\rho(\mathbf{r})] + \frac{\hbar^2}{2\,m_{\rm Li}} \int d\mathbf{r}\,|\nabla\Psi^{gs}(\mathbf{r})|^2 + \int\int d\mathbf{r}\,d\mathbf{r}'\,|\Psi^{gs}(\mathbf{r})|^2\,V_{X^2\Sigma}(|\mathbf{r}-\mathbf{r}'|)\,\rho(\mathbf{r}').$$

We have self-consistently solved the equations that result from the variations of E with respect to Ψ^{gs} and $\rho(\mathbf{r})$ [19].

Figure 2 displays the structure of two typical Li@He$_N$ drops corresponding to $N = 1,000$, showing that the Li atom sits at the surface of the drop producing a more pronounced dimple for ^{3}He than

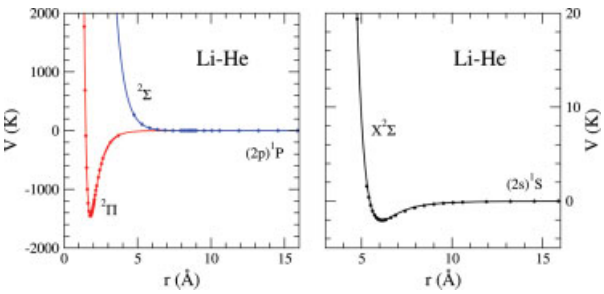

FIGURE 1. Li–He pair potentials. The dots are the calculated values, and the lines are the result of the fits. [Color figure can be viewed in the online issue, which is available at wileyonlinelibrary.com.]

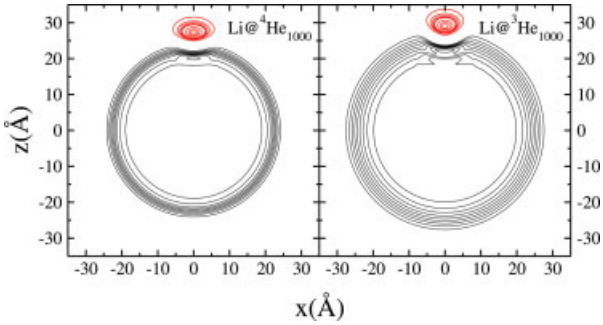

FIGURE 2. Helium equidensity lines on a plane of symmetry of the Li-drop complex corresponding to nine values between $0.1\rho_b$ and $0.9\rho_b$ in $0.1\rho_b$ steps, with ρ_b being the liquid density at 0 K, namely, 0.0218 Å^{-3} for ^{4}He and 0.0163 Å^{-3} for ^{3}He. Also shown are several equiprobability density lines of Li between $0.001 \times \max\{|\Psi^{gs}|^2\}$ and $0.99 \times \max\{|\Psi^{gs}|^2\}$. Left panel: Li@^{4}He$_{1,000}$. Right panel: Li@^{3}He$_{1,000}$. [Color figure can be viewed in the online issue, which is available at wileyonlinelibrary.com.]

for ^{4}He. This is an intuitive result, as the surface tension of liquid ^{4}He is 0.274 K Å^{-2}, whereas that of liquid ^{3}He is 0.113 K Å^{-2}. For a given N, the ^{3}He$_N$ drop is larger than the ^{4}He$_N$ one because the bulk liquid density ρ_b of ^{3}He is about 25% smaller than that of ^{4}He, and the radius of the drop, defined as the radius at which the drop density equals $\rho_b/2$, is $R = r_0 N^{1/3}$, with $r_0 = [3/(4\pi\rho_b)]^{1/3}$. We have checked that the structure of the doped drops is very similar to that previously obtained [12, 17] using the Li–He $X^2\Sigma$ potential calculated by Patil [28].

The absorption spectrum around the $2p \leftarrow 2s$ transition has been obtained from the equilibrium helium density and impurity wave function employing the two different approaches mentioned in the Introduction section. Within the DIM approach, using the Born-Oppenheimer approximation to factorize the electronic and nuclear wave functions, along with the Franck-Condon approximation by which the positions of the atomic nuclei are kept frozen during the transition, the line shape for an electronic transition from the ground state (gs) to the excited state (ex) can be calculated as the Fourier transform of the time-correlation function

$$I(\omega) \propto \sum_m \int dt\, e^{-i(\omega+\omega^{gs})t} \times \int d^3\mathbf{r}\,\Psi^{gs}(\mathbf{r})^* e^{(it/\hbar)H_m^{ex}}\,\Psi^{gs}(\mathbf{r}), \quad (2)$$

where $\hbar\omega^{gs}$ is the eigenenergy of Li in its ground state. The Hamiltonian in the time evolution operator $e^{(it/\hbar)H_m^{ex}}$ is defined as $H_m^{ex} = T + V_m^{ex}(\mathbf{r})$, where T

is the kinetic energy operator and $V_m^{\rm ex}(\mathbf{r})$ is the PES defined by the mth eigenvalue of the excited potential matrix $V_T(\mathbf{r}) = U(\mathbf{r}) + V_{\rm SO}$, where $U(\mathbf{r})$ is the convolution of the excited pair potentials $^2\Pi$ and $^2\Sigma$ with the helium density $\rho(\mathbf{r})$, whereas $V_{\rm SO}$ accounts for the spin-orbit coupling [19].

Introducing in Eq. (2) $\Psi^{\rm gs}(\mathbf{r}) = \sum_\nu a_\nu^m \Psi_\nu^m(\mathbf{r})$, where $\Psi_\nu^m(\mathbf{r})$ are the eigenfunctions of $H_m^{\rm ex}$ and $a_\nu^m = \int d^3\mathbf{r}\, \Psi_\nu^m(\mathbf{r})^* \Psi^{\rm gs}(\mathbf{r})$ are the Franck-Condon factors, we obtain

$$I(\omega) \propto \sum_m \int dt\, e^{-i(\omega+\omega^{\rm gs})t} \sum_\nu |a_\nu^m|^2 e^{i\omega_\nu^m t} = \sum_m \sum_\nu |a_\nu^m|^2 \delta(\omega + \omega^{\rm gs} - \omega_\nu^m), \quad (3)$$

where $\hbar\omega_\nu^m$ are the eigenvalues of $H_m^{\rm ex}$.

When the Franck-Condon factors arise from the overlap between the ground and excited states with large quantum numbers, we can assume that $\langle T\rangle \ll \langle V_m^{\rm ex}\rangle$, and the Hamiltonian is approximated by $H_m^{\rm ex} \sim V_m^{\rm ex}(\mathbf{r})$. Introducing this approximation in Eq. (2) and integrating over time one obtains a semiclassical expression for $I(\omega)$

$$I(\omega) \propto \sum_m \int d^3\mathbf{r}\, |\Psi^{\rm gs}(\mathbf{r})|^2 \delta\left[\omega - \left(V_m^{\rm ex}(\mathbf{r})/\hbar - \omega^{\rm gs}\right)\right]. \quad (4)$$

We have recently proposed a straightforward method [20] to evaluate this expression using a DF sampling simulation inspired by that proposed in [29]. This simulation models the coupling between the impurity excitation and the vibrations of the helium cavity around it, substantially contributing to the broadening of the absorption peak and improving the agreement with the experiment. During the sampling simulation, and due to the Li light mass, the use of the eigenvalue $\hbar\omega^{\rm gs}$ for the ground state energy was found to be more appropriate, instead of the pairwise sum described in [20]. A similar improvement was introduced by Cheng and Whaley in their calculations on the absorption spectrum of Li in solid H_2 [30] (see also [13]).

Absorption Spectrum

Figure 3 shows the calculated absorption spectra using the semiclassical method compared to the experimental results [12]. It can be seen that the shift with respect to the free atomic lines is small and that the linewidths are underestimated, as also found by other authors [12, 13]. Part of the underestimation could be fixed by allowing the Li atom to wander in the dimple due to thermal effects not taken into account [19, 31].

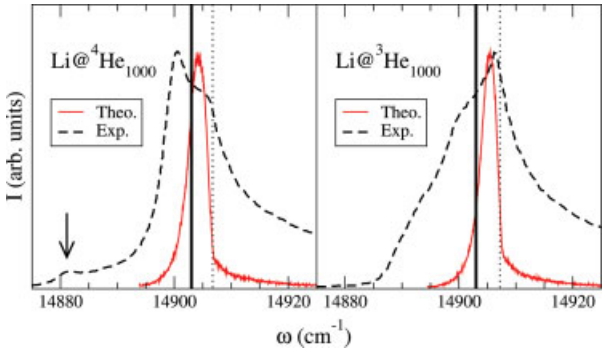

FIGURE 3. Left panel: Absorption spectrum (arbitrary units) for Li@^{4}He$_{1,000}$. The theoretical result has been obtained using the semiclassical approach by adding the $^2\Sigma_{1/2}$, $^2\Pi_{1/2}$, and $^2\Pi_{3/2}$ contributions, and normalized so that the experimental and theoretical peaks have the same height. The vertical thick lines indicate the location of the absorption lines of the free Li atom, and the vertical dotted lines indicate the energy at which the contribution of the bound-free transitions starts dominating. The red-shifted shoulder is indicated by an arrow. Right panel: Same as left panel for Li@^{3}He$_{1,000}$. In both cases, the experimental result [12] corresponds to $N \sim 5,000$. [Color figure can be viewed in the online issue, which is available at wileyonlinelibrary.com.]

As indicated, the semiclassical approach properly describes the transition to excited states with large quantum numbers, which in our case correspond to high energy free states, i.e., bound-free transitions. However, it is unable to reproduce bound–bound transitions since the discrete nature of the excited-state Hamiltomian is replaced by a continuous potential energy surface. For Li, the contribution of the $^2\Pi_{1/2}$ and $^2\Pi_{3/2}$ PES is strongly dominated by bound–bound transitions, and the semiclassical approach misses the interesting experimental finding that for ^{4}He, the main peak in the absorption line is red-shifted instead of blue-shifted, as it happens for ^{3}He. On the contrary, the contribution of the $^2\Sigma_{1/2}$ PES transitions is of bound-free type and the long tail in the blue-shifted region of the spectrum is well reproduced. As can be seen from Figure 3, this happens for both ^{4}He and ^{3}He droplets.

The previous discussion stresses the importance of a full quantum treatment for describing the Li absorption line. Figure 4 shows the main result of this work, namely the absorption spectrum calculated from the Fourier transform of the time-correlation function, Eq. (3). For both ^{4}He and ^{3}He droplets,

more than 99% of the overlap of the Li gs wave function with vibrational states of the $^2\Pi_{1/2}$ and $^2\Pi_{3/2}$ PES corresponds to bound–bound transitions. On the contrary, the overlap with states of the $^2\Sigma_{1/2}$ PES yields bound-free contributions which generate a continuous, long blue-shifted tail. This produces a characteristic Li spectrum, with a conspicuous peak structure that does not appear in any other alkali atom, see Figure 4.

In the case of ^{4}He droplets, the dimple structure is such that it yields $^2\Pi_{1/2}$ and $^2\Pi_{3/2}$ PES deeper than the ground state $X^2\Sigma$ PES. Hence, the main bound–bound transitions are red-shifted with respect to the gas phase ones, and they lie away from the bound-free tail (left panel in Figure 4). In contradistinction, the dimple structure in ^{3}He droplets yields a $^2\Pi_{3/2}$ PES shallower than the ground state PES, producing the intense blue-shifted peak close to the bound-free tail displayed in the right panel of Figure 4. We display in Figure 5 the $X^2\Sigma$ and $^2\Pi_{3/2}$ PES cut along the z-axis, each one referred to its asymptotic limit, to explicitly show this effect. The $^2\Pi_{1/2}$ PES transitions are red-shifted for ^{3}He and ^{4}He droplets as well. These facts qualitatively explain the main features of the experimental spectrum of Li in helium drops: a long blue tail and an intense peak, red-shifted in the ^{4}He case, and blue-shifted in the ^{3}He case.

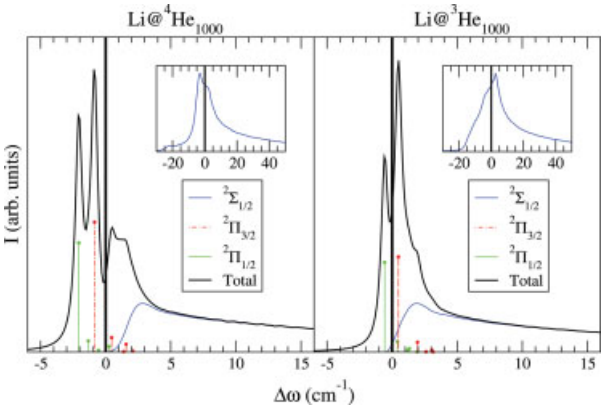

FIGURE 4. Left panel: Absorption spectrum (arbitrary units) for Li@^{4}He$_{1,000}$ obtained using the Fourier transform of the time-correlation function. The experimental spectrum is shown in the inset. The more intense bound–bound transitions are represented by dot-topped lines. These lines have been convoluted with a Lorenzian with a full width at half maximum of 0.6 cm^{-1}. This value has been fixed rather arbitrarily. The vertical thick line indicates the location of the absorption lines of the free Li atom. Right panel: same as left panel for Li@^{3}He$_{1,000}$. [Color figure can be viewed in the online issue, which is available at wileyonlinelibrary.com.]

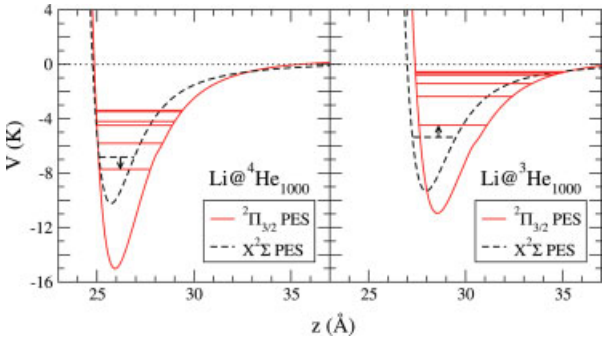

FIGURE 5. $X^2\Sigma$ and $^2\Pi_{3/2}$ PES cut along the z-axis, each one referred to its asymptotic limit. These PES have been obtained by convoluting the corresponding Li–He pair potential with the ground-state helium density. Left panel: Li@^{4}He$_{1,000}$; right panel: Li@^{3}He$_{1,000}$. The main transition is represented by an arrow connecting the ground-state of Li in the $X^2\Sigma$ PES with the lowest lying state of Li in the $^2\Pi_{3/2}$ PES. Also shown are the first excited states of Li in the $^2\Pi_{3/2}$ PES. [Color figure can be viewed in the online issue, which is available at wileyonlinelibrary.com.]

We want to stress that the apparent splitting of the two $^2\Pi$ peaks is not a spin-orbit effect (recall that the splitting of the doublet lines of Li in the gas phase is very small, $\sim$0.34 cm^{-1}). It is due to the delocalization of the impurity in a very anisotropic helium environment, and appears even for impurities such as Ca(^{1}S) for which there is no spin-orbit splitting [19]. Because the dimple is broader for ^{4}He than for ^{3}He (see Fig. 1), the delocalization is enhanced for the former, as it allows for a wider lateral motion of Li. This increases the splitting further, eventually explaining the appearance of a red-shifted shoulder in ^{4}He and not in ^{3}He. This feature of the experimental spectrum is only very qualitatively reproduced by our calculations, as in the case of Na, for which we have also found a sizeable bound-free contribution from the Π symmetry PES [20]. For heavier alkali atoms, their large mass hinders the zero point motion and quenches the overlap with excited vibrational states, so that no red-shifted shoulder appears in the experimental absorption lines [12].

Summary

We have studied the dipole absorption line of Li atoms attached to helium droplets using a full three-dimensional approach and the Fourier analysis of the time-correlation function of the impurity. Both ingredients are instrumental to properly address the

absorption spectrum of the lightest alkali atom and, to the best of our knowledge, they have not been included simultaneously in previous calculations. We have shown that the semiclassical approximation misses the main features that distinguish the line shape in ^{4}He and ^{3}He droplets.

The absorption spectrum of Li attached to helium drops is strongly dominated by quite a few bound–bound transitions and a continuous of bound-free trasitions that generate a long blue-shifted tail. These bound–bound contributions arise from electronic "jumps" from the $X^2\Sigma$ to the $^2\Pi_{1/2}$ and $^2\Pi_{3/2}$ PES.

The underestimation of the absorption linewidth in the case of the lighter alkali Na and especially of Li atoms, might be likely attributed to thermal effects not taken into consideration. We want to recall that the average size of the drops in the experiments is about $N = 5,000$, whereas our calculations have been carried out for $N = 1,000$. Simulating bigger drops would essentially yield a broader absorption line [20]. This is expected to little affect Li in a $N = 1,000$ droplet, as this impurity sits at the outer surface of the droplet and curvature effects are already small for such a large system.

The different structure of the dimple in ^{4}He and ^{3}He droplets, less marked in the former than in the latter, is the sole ingredient in the calculation of the absorption spectrum that turns out to be different for both isotopes, and it has two effects on the absorption line. On the one hand, the Li atom is more delocalized laterally in ^{4}He than in ^{3}He droplets, explaining the appearance of a red-shifted shoulder in the ^{4}He case. On the other hand, it causes that the relative position of the $^2\Pi_{3/2}$ PES with respect to the $X^2\Sigma$ PES in either helium isotope are opposite, yielding a main peak that is red-shifted with respect to the free atomic lines for ^{4}He droplets, and blue-shifted for ^{3}He droplets.

The present work, together with, the previous ones on other alkali and alkaline earth impurities in helium drops, shows the suitability of the DF approach to even reproduce detailed features of their absorption spectrum as found by electronic spectroscopy. To achieve such an accurate description, it is crucial to have available precise helium-impurity pair potentials.

References

1. Harms, J.; Hartmann, M.; Toennies, J. P.; Vilesov, A. F.; Sartakov, B. J Mol Spectrosc 1997, 185, 204.
2. Hartmann, M.; Mielke, F.; Toennies, J. P.; Vilesov, A. F.; Benedek, G. Phys Rev Lett 1996, 76, 4560.
3. Stienkemeier, F.; Vilesov, A. F. J Chem Phys 2001, 115, 10119.
4. Toennies, J. P.; Vilesov, A. F. Angew Chem Int Ed Engl 2004, 43, 2622.
5. Stienkemeier, F.; Lehmann, K. K. J Phys B 2006, 39, R127.
6. Tiggesbäumker, J.; Stienkemeier, F. Phys Chem Chem Phys 2006, 9, 4748.
7. Stienkemeier, F.; Higgins, J.; Callegari, C.; Kanorsky, S. I.; Ernst, W. E.; Scoles, G. Z Phys D 1996, 38, 253.
8. Brühl, F. R.; Trasca, R. A.; Ernst, W. E. J Chem Phys 2001, 115, 10220.
9. Bünermann, O.; Mudrich, M.; Weidemüller, M.; Stienkemeier, F. J Chem Phys 2004, 121, 8880.
10. Stienkemeier, F.; Bünermann, O.; Mayol, R.; Ancilotto, F.; Barranco, M.; Pi, M. Phys Rev B 2004, 70, 214509.
11. Mayol, R.; Ancilotto, F.; Barranco, M.; Bünermann, O.; Pi, M.; Stienkemeier, F. J Low Temp Phys 2005, 138, 229.
12. Bünermann, O.; Droppelmann, G.; Hernando, A.; Mayol, R.; Stienkemeier, F. J Phys Chem A 2007, 111, 12684.
13. Nakayama A.; Yamashita, K. J Chem Phys, 2001, 114, 780.
14. Ancilotto, F.; Cheng, E.; Cole, M. W.; Toigo, F. Z Phys B 1995, 98, 323.
15. Guardiola, R.; Navarro, J.; Mateo, D.; Barranco, M. J Chem Phys 2009, 131, 174110.
16. de Lara-Castells, M. P.; Villarreal, P.; Delgado-Barrio, G.; Mitrushchenkov, A. O. J Chem Phys, 2009, 131, 194101.
17. Barranco, M.; Guardiola, R.; Hernández, E. S.; Mayol, R.; Navarro, J.; Pi, M. J Low Temp Phys 2006, 142, 1.
18. Ellison, F. O. J Am Chem Soc 1963, 85, 3540.
19. Hernando, A.; Barranco, M.; Mayol, R.; Pi, M.; Krośnicki, M. Phys Rev B 2008, 77, 024513.
20. Hernando, A.; Barranco, M.; Mayol, R.; Pi, M.; Ancilotto, F.; Bünermann, O.; Stienkemeier, F. J Low Temp Phys 2010, 158, 105.
21. Dalfovo, F.; Lastri, A.; Pricaupenko, L.; Stringari, S.; Treiner, J. Phys Rev B 1995, 52, 1193.
22. Barranco, M.; Guilleumas, M.; Hernández, E. S.; Mayol, R.; Pi, M.; Szybisz, L. J Low Temp Phys 2004, 136, 139.
23. Kerkines, I. S. K.; Mavridis, A. J Phys Chem A 2000, 104, 408.
24. Kerkines, I. S. K.; Mavridis, A. J Chem Phys 2002, 116, 9305.
25. Dunning, H. T., Jr. J Chem Phys 1989, 90, 1007.
26. Woon, D. E.; Dunning, H. T., Jr. J Chem Phys 1994, 100, 2975.
27. (a) Aziz, R. A.; Nain, V. P. S.; Caley, J. S.; Taylor, W. L.; McConville, G. T. J Chem Phys 1979, 70, 4330; (b) Aziz, R. A.; McCourt, F. R. W.; Wong, C. C. K. Mol Phys 1987, 61, 1487.
28. Patil, S. H. J Chem Phys 1991, 94, 8089.
29. Nakatsukasa, T.; Yabana, K.; Bertsch, G. F. Phys Rev A 2002, 65, 032512.
30. Cheng, E.; Whaley, K. B. J Chem Phys 1996, 104, 3155.
31. Hernando, A.; Barranco, M.; Mayol, R.; Pi, M.; Ancilotto, F. Phys Rev B 2008, 78, 184515.